

Structure and Spin Dynamics of $\text{La}_{0.85}\text{Sr}_{0.15}\text{MnO}_3$

L. Vasiliu-Doloc^{1,2}, J. W. Lynn^{1,2}, A.H. Moudden³, A.M. de Leon-Guevara⁴ and A. Revcolevschi⁴

¹*NIST Center for Neutron Research, National Institute of Standards and Technology, Gaithersburg, Maryland 20899*

²*Center for Superconductivity Research, University of Maryland, College Park, MD 20742*

³*Laboratoire Léon Brillouin, CEA-CNRS, CE/Saclay, 91191 Gif sur Yvette Cedex, France*

⁴*Laboratoire de Chimie des Solides, Université Paris-Sud, 91405 Orsay, France*

Neutron scattering has been used to study the structure and spin dynamics of $\text{La}_{0.85}\text{Sr}_{0.15}\text{MnO}_3$. The magnetic structure of this system is ferromagnetic below $T_C \simeq 235$ K. We see anomalies in the Bragg peak intensities and new superlattice peaks consistent with the onset of a spin-canted phase below $T_{CA} \sim 205$ K, which appears to be associated with a gap at $q = (0, 0, 0.5)$ in the spin-wave spectrum. Anomalies in the lattice parameters indicate a concomitant lattice distortion. The long-wavelength magnetic excitations are found to be conventional spin waves, with a gapless (< 0.02 meV) isotropic dispersion relation $E = Dq^2$. The spin stiffness constant D has a $T^{5/2}$ dependence at low T , and the damping at small q follows $q^4 T^2$. An anomalously strong quasielastic component, however, develops at small wave vector above ~ 200 K and dominates the fluctuation spectrum as $T \rightarrow T_C$. At larger q , on the other hand, the magnetic excitations become heavily damped at low temperatures, indicating that spin waves in this regime are not eigenstates of the system, while raising the temperature dramatically increases the damping. The strength of the spin-wave damping also depends strongly on the symmetry direction in the crystal. These anomalous damping effects are likely due to the itinerant character of the e_g electrons.

INTRODUCTION

The correlated dynamics of spins and charges near the Mott transition in doped lanthanum manganites $\text{La}_{1-x}\text{A}_x\text{MnO}_3$ ¹ has generated continued interest, both because these systems exhibit anomalously large magnetoresistance effects near the Curie temperature^{2,3}, and because the physics of this class of materials is related to the high- T_c superconducting copper oxides. Like the cuprates, these materials are in the vicinity of an insulator-metal transition, as well as magnetic and structural instabilities, while to date no superconductivity has been found. Rather, they exhibit exotic properties such as a dramatic increase in the conductivity when the system orders ferromagnetically, either by cooling in temperature or by applying a magnetic field. It has been suggested that an understanding of these materials must include, in addition to the double exchange mechanism⁴ and strong electron correlations², a strong electron-phonon interaction⁵. Cooperative Jahn-Teller (JT) distortions associated with the Mn^{3+} JT ions have been evidenced from structural studies at low doping, where the system is insulating and antiferromagnetic, and may be an important contribution to orbital ordering, double exchange, and related spin ordering and transport properties observed at higher concentrations. As the doping concentration x increases, the static JT distortion weakens progressively and the system becomes metallic and ferromagnetic. It is believed that in the absence of a cooperative effect in this regime, local JT distortions persist on short time and length scales. These short-range correlations, together with the electron correlations, would create the effective carrier mass necessary for large magnetoresistance. The existence of strong electron correlations is expected to affect the magnetic order-

ing and the magnetic excitation spectrum, and thus the spin dynamics can provide crucial information for determining the itinerancy of the system and the importance of the electron correlations.

A number of inelastic neutron scattering studies of the spin dynamics has been carried out in these systems, but most of them were carried out either in the strongly-doped regime, or in the lightly-doped limit, and only a few of them investigated the spin-wave dispersion to the zone boundary⁶⁻⁹. These studies suggested essentially standard spin dynamics of a conventional metallic ferromagnet, except for the Ca-doped samples⁸ and, more recently, for $\text{Nd}_{0.7}\text{Sr}_{0.3}\text{MnO}_3$ and $\text{Pr}_{0.7}\text{Sr}_{0.3}\text{MnO}_3$,¹⁰ where coexistence of spin-wave excitations and a spin diffusion component was observed in the ferromagnetic phase. Perring et al.⁹ used pulsed neutron scattering to measure the spin-wave dispersion throughout the Brillouin zone of $\text{La}_{0.7}\text{Pb}_{0.3}\text{MnO}_3$, and concluded that a simple isotropic Heisenberg Hamiltonian with only nearest-neighbor coupling could account for the entire dispersion relation. They did not observe any intrinsic linewidths at low temperature, possibly because of the coarse resolution needed to observe the high energy spin waves. They did observe, however, an unusual broadening of the high-energy spin waves at elevated temperatures.

At the other end of the (x, T) phase diagram, the system is semiconducting for low doping concentrations, with a canted spin structure^{11,12}. The spin dynamics are highly anisotropic and are described by a strong in-plane ferromagnetic exchange coupling and a weak out-of-plane antiferromagnetic coupling. The ferromagnetic coupling in this limit results from orbital ordering in agreement with Goodenough-Kanamori rules. Substituting La with Sr introduces doped holes in the system, but also lattice distortions that modify the overlap of the orbitals. Thus

a clear competition arises between the orbital-ordering inducing antiferromagnetic or ferromagnetic correlations and the double exchange mechanism, which favors ferromagnetic correlations. It is therefore of great interest to elucidate the crossover mechanism from the weakly-doped to the strongly-doped limit. In the intermediate doping regime we expect to see a strong deviation from the double-exchange model prediction for the spin wave spectrum.

So far, no results on the spin dynamics in the intermediate doping regime have been reported. We have therefore concentrated on $\text{La}_{0.85}\text{Sr}_{0.15}\text{MnO}_3$. We find that the long-wavelength magnetic excitations are conventional spin waves at low T , while for $T \rightarrow T_C$ an anomalously strong quasielastic component develops at small wave vectors and dominates the fluctuation spectrum. In the large wave vector regime very large intrinsic linewidths develop with increasing q in the ground state of this system, and we find that the strength of this damping depends strongly on the symmetry direction in the crystal. This demonstrates that conventional magnons are not eigenstates of this system at large q , which is in contradiction to the expectations for a standard Heisenberg model, or a simple one-band, fully-polarized double exchange (half-metallic) ferromagnet. We also find that increasing the temperature dramatically reduces the lifetime of the large- q magnetic excitations, indicating that there are strongly temperature-dependent contributions to the spin-wave damping as well. These anomalous damping effects are likely due to the itinerant character of the e_g electrons. From the structural point of view, we observe anomalies in the Bragg peak intensities accompanied by the appearance of superlattice peaks indexed with respect to the orthorhombic $Pbnm$ cell as $(0\ 0\ l)$ with $l=\text{odd}$ or $(h\pm 1/2, k\pm 1/2, 0)$ in related twin domains. These are consistent with the onset of a spin-canted phase below $T_{CA} = 205$ K, as previously suggested by Kawano et al.¹³. The superlattice peaks are extremely weak, indicating that this subtle distortion of the magnetic structure can be treated as a small perturbation of the purely ferromagnetic arrangement. Anomalies in the lattice parameters indicate a concomitant structural distortion. Other strong superlattice peaks, indexed as $(h, k, l\pm 1/2)$ or $(h\pm 1/4, k\pm 1/4, 0)$ in related twin domains, have been reported by Yamada et al., and interpreted as the manifestation of a polaron lattice that would form below 190 K. We did not observe such strong peaks in our $x = 0.15$ sample using neutron scattering, but we did observe weak and broad peaks using synchrotron X-ray scattering, which in addition presented strong irradiation effects. A comprehensive analysis of these superlattice peaks is in progress¹⁴. We note that preliminary results of our studies have been reported previously^{15,16}.

EXPERIMENT

The single crystal of $\text{La}_{0.85}\text{Sr}_{0.15}\text{MnO}_3$ used in the present inelastic neutron scattering experiments was

grown in Laboratoire de Chimie des Solides, Orsay, France, using the floating zone method. The crystal is 5-6 mm in diameter and 3 cm in length and weighs 6.5 grams. It was oriented such that the [010] and [001] axes of the orthorhombic $Pbnm$ cell lie in the scattering plane. The inelastic measurements reported here were performed on the BT-2, BT-4, BT-9 (thermal beam) and NG-5 (cold source) triple-axis spectrometers at the NIST research reactor. In order to reduce extinction effects, the diffraction experiments were carried out on a much smaller single crystal weighing 0.3 g, grown under the same conditions. In all cases pyrolytic graphite (PG) (0 0 2) has been used as an analyzer. As monochromator, the same reflection was used on the BT-2, BT-9 and NG-5 spectrometers, while the copper (2 2 0) reflection was used on BT-4 to investigate the higher energy excitations. Either PG or cold Be filters were used as appropriate, along with a variety of collimator combinations.

STRUCTURE AND MAGNETIC ORDER

$\text{La}_{0.85}\text{Sr}_{0.15}\text{MnO}_3$ has a high-temperature rhombohedral phase ($R\bar{3}c$), and undergoes a structural phase transition at $T_S = 360$ K to an orthorhombic phase ($Pbnm$), as shown in Fig. 1(a). In the paramagnetic phase the resistivity of this system initially increases with decreasing temperature^{17,18}, but then shows an abrupt drop associated with the onset of ferromagnetic long-range order at $T_C = 235$ K, as confirmed by magnetization measurements versus T obtained from Bragg scattering (see Fig. 1(b)). At a lower temperature around 205 K, the resistivity exhibits a fairly sharp upturn accompanied by anomalies in the Bragg peak intensities and the appearance of superlattice peaks, consistent with a subtle distortion of the magnetic structure below $T_{CA} \simeq 205$ K¹³ and a possible structural distortion¹⁴, as described below. These superlattice peaks are weak, arising from a small perturbation of the FM structure, and thus from the dynamical point of view this system is a ferromagnet to a good approximation throughout the magnetically ordered state.

The integrated intensity of the (0 2 0) ferromagnetic Bragg reflection as a function of temperature is shown in Fig. 1(b) (closed squares). This reflection has a weak nuclear structure factor, and therefore has a small intensity in the paramagnetic phase. Below T_C , magnetic scattering due to the ferromagnetism of spins aligning on the manganese atoms produces a magnetic structure factor and results in an increase of intensity. The data in Fig. 1(b) are the same on warming and on cooling, with no visible hysteresis. It is thus very likely that this ferromagnet exhibits a second-order phase transition. Nevertheless, these data cannot be used to extract a critical magnetic exponent β , because of the anomaly we see below 210 K. There is a loss of intensity in the (0 2 0) reflection which coincides, on one hand, with the upturn in the resistivity and, on the other hand, with the appearance of weak superlattice peaks at antiferromagnetic Bragg points along the c direction, such as the (0 0 3) reflection, also repre-

sented in Fig. 1(b) (closed circles). Note the factor of ten difference in intensity scales, with the $(0\ 0\ 3)$ intensity being more than an order of magnitude lower in strength. In the $Pbnm$ symmetry, $(0\ 0\ l)$ nuclear reflections with $l=\text{odd}$ are not allowed, and we see in Fig. 2 that there is no significant scattering present at $Q = (0\ 0\ 3)$ at 215 K. The appearance of such new reflections indicates that a second phase transition occurs at $T \sim 205$ K, of magnetic and/or structural nature. We can readily discard the possibility that the Bragg peaks at $(0\ 0\ l)$ with $l=\text{odd}$ come from a second, distinct phase present in the sample, because the 205 K transition is also evident in the $(0\ 2\ 0)$ reflection. These data are consistent with the onset of a canted spin structure at 205 K. Indeed, the canting of spins would result in a small antiferromagnetic moment at the expense of a reduction in the ferromagnetic moment (see Fig. 3). We estimate the cant angle to be $9.4^\circ \pm 0.8^\circ$. In the double exchange model holes can only hop if adjacent spins are aligned, and the onset of ferromagnetism at 235 K gives rise to a metallic-like behavior of the resistivity. At 205 K, a residual superexchange interaction (left over from the low-doping limit) cants the spins away from the perfect ferromagnetic arrangement. The AF component suppresses the metallic state by reducing the matrix elements of electron hopping between Mn sites, thus explaining the upturn in the resistivity. A similar behavior has been observed for $x=0.1$ and 0.125 .¹³ The new type of magnetic long range order that occurs below T_{CA} appears to be accompanied by the opening of a small gap at $q = (0, 0, 0.5)$ in the spin-wave spectrum, and by a lattice distortion as described below.

Figure 1(a) shows the integrated intensity of the $(1\ 2\ 0)$ nuclear Bragg reflection, which is allowed only in the orthorhombic symmetry. Therefore, there is no intensity observable on cooling until $T_S \sim 360$ K, where a sharp increase occurs when the system undergoes the rhombohedral-to-orthorhombic structural phase transition. Upon cooling further, we see that the intensity of the $(1\ 2\ 0)$ reflection starts decreasing at $T_C = 235$ K, reaches a local minimum at T_{CA} , and then starts increasing again. This break in the intensity of the $(1\ 2\ 0)$ reflection corresponds closely to the anomaly in the ferromagnetic $(0\ 2\ 0)$ peak and indicates a coupling between the magnetic system and the lattice. Therefore, the new type of magnetic order that appears at T_{CA} is accompanied by a lattice distortion, also evident in anomalies of the lattice parameters, as shown in Fig. 4(a). The a and b lattice parameters determined from single-crystal diffraction are shown vs. T in Fig. 4. Above T_C , the difference between a and b is large, indicating that the system is in the distorted-perovskite orthorhombic O' phase. Upon approaching T_C , both a and b start decreasing abruptly, but have opposite variations below T_C , with a maximum in a and a minimum in b half way between T_C and T_{CA} . Below 200 K the difference between a and b becomes very small, suggesting that the system releases the lattice distortions and goes into the undistorted-perovskite orthorhombic O^* phase. Due to the uncertainty in assign-

ing a and b from single-crystal diffraction on a twinned sample, it is possible that the situation described in Fig. 4(b) is realized, where there is a crossover between a and b at T_C . In this case, upon approaching T_C , a increases and b decreases sharply, they cross at T_C , and continue their variation with the same slope until they reach a maximum and a minimum, respectively, before their variation changes sign. The upturn in resistivity coincides with T_{CA} and with the lower structural transition temperature to the O^* phase where a and b become equal, the same as observed for the $x=0.125$ system¹⁹. But unlike the structural phase diagram proposed by Kawano et al.¹⁹, we find the $x=0.15$ system to be in the O' phase above T_C , not in the O^* phase. It is clear so far that the $\text{La}_{1-x}\text{Sr}_x\text{MnO}_3$ system in the concentration range $0.10 \leq x \leq 0.17$ is in the vicinity of structural and magnetic instabilities. This only makes it more difficult to sort out all the subtleties of the magnetic and structural phase diagram in this region, and further work may be needed to produce a reliable phase diagram for this system, for example by exploring a fine mesh of concentrations instead of drawing conclusions based on the study of a few selected doping levels.

The resistivity upturn for the $x = 0.10$ and 0.15 systems has been associated by Yamada et al.²⁰ with the onset of a polaron ordered phase with the periodicity $2a \times 2b \times 4c$ in the cubic perovskite cell. These authors have based their conclusion on the observation of superlattice peaks indexed as $(h \pm 1/4, k \pm 1/4, 0)$ or $(h, k, l \pm 1/2)$ in a multidomain crystal composed of microtwins. We have carried out a thorough search for such superlattice peaks using neutron scattering and have not found any. Therefore, we cannot confirm the model proposed by Yamada et al. It is possible that this disagreement arises from slightly different nominal compositions and/or from the difficulty to index the numerous reflections in a multidomain crystal, as the one used by Yamada et al. The possible existence of phases with compositional modulations in single crystals grown using different techniques, or a short range order of the doping element itself, could produce superlattice peaks as well. It is also known that these materials can easily incorporate vacancies which could lead to ordered defects. Using synchrotron X-ray scattering we observed weak and broad superlattice peaks at the positions indicated by Yamada et al., suggestive of a short-range order in the system, but it necessitated the high flux from a synchrotron source to reveal them. The doping range $0.10 \leq x \leq 0.17$ is a critical concentration regime in the sense that the magnetic and nuclear structure vary rapidly with x . Nevertheless, the average nuclear structure of this system has been well established. This is why it is surprising that Yamada et al. present data showing $(1\ 0\ 0)$ reflections in the orthorhombic phase of their samples, much stronger than the $(2\ 0\ 0)$ reflection. In the orthorhombic $Pbnm$ symmetry this type of reflection is not allowed.

In conclusion, we believe that the upturn in the resistivity corresponds to the onset of an AF component at

T_{CA} . We emphasize that the AF component is small, arising from a small perturbation of the FM structure, and thus the spin dynamics of the $x=0.15$ system of present interest can be treated to a good approximation as a ferromagnet throughout the magnetically ordered phase.

SPIN DYNAMICS

a) Small wave vector regime

We have investigated the spin dynamics in the (0,1,0) and (0,0,1) high-symmetry directions of the orthorhombic unit cell. The ground state spin dynamics for a half-metallic ferromagnet was not expected to differ much from the conventional picture of well defined spin waves, and we found that the long wavelength magnetic excitations were in fact the usual hydrodynamic spin waves, with a dispersion relation given by $E = E_0 + Dq^2$, where E_0 is the spin-wave energy gap and D is the spin stiffness constant. In order to set an upper limit on the value of any energy gap E_0 , we have performed very high-resolution inelastic measurements on the NG-5 (SPINS) cold-neutron triple-axis spectrometer. Figure 5(a) illustrates the measured spin-wave dispersion relation along the (0,0,1) direction at 10 K and 220 K. The spin-wave energies have been obtained from least-squares fits of the data to the dispersion relation convoluted with the instrumental resolution. The solid curves are fits to $E = E_0 + Dq^2$. The fitted value of E_0 at 10 K is 0.019 ± 0.04 meV, where the quoted error includes only statistical errors. The negligible value of E_0 indicates that this material is a prototypical isotropic ferromagnet, comparable to the soft amorphous ferromagnets. Previous studies have shown that the undoped system is a Jahn-Teller distorted perovskite that consists of sheets of ferromagnetic spins in the ab plane that are coupled antiferromagnetically along the c -axis. The spin-wave energy gap is ~ 2.5 meV for $x=0$, and then decreases continuously with x and becomes zero for $x \simeq 0.1$ as the antiferromagnetic c -axis interaction changes sign and becomes ferromagnetic^{11,12}. The present measurements confirm that $x=0.15$ belongs to the ferromagnetic doping concentration range for which the spin-wave energy gap is essentially zero. The fitted values for the spin stiffness constant D are 94.87 ± 1.18 meV \AA^2 at 10 K, and 40.53 ± 0.13 meV \AA^2 at 220 K. The low-temperature value of the spin stiffness constant gives a ratio of $D/k_B T_c \sim 4.6 \text{ \AA}^2$. We can also see that energies for $q > 0.15$ depart from the q^2 -dependence, as higher-order terms in the power law expansion of the dispersion relation become significant, as expected.

Similar data have been obtained along the (0,1,0) direction, and Fig. 5(b) plots the temperature dependence of the stiffness D in both directions. This result shows that the exchange interactions (as estimated from the long-wavelength spin dynamics) are remarkably isotropic, and demonstrates again that the dimen-

sional crossover from the 2D-like planar ferromagnetic (in the A-type AF ordering) to the 3D isotropic ferromagnetic character takes place at concentrations lower than $x=0.15$, probably $x \sim 0.1$,^{11,12} where the system still behaves like a semiconductor. It is thus interesting to note that the metallic ferromagnetic features in the spin dynamics appear at lower doping concentrations than the compositional insulator-metal transition at $x \sim 0.17$, above which the canting transition is no longer observed at any T . This observation supports the conjecture that the insulator-metal phase boundary is actually located at $x=0.1$ in the $\text{La}_{1-x}\text{Sr}_x\text{MnO}_3$ system, but the AF component suppresses the metallic state in samples with $0.1 \leq x \leq 0.15$, without having a strong influence on the character of the spin dynamics.

The long-wavelength spin wave data can be compared to the Dyson formalism of two-spin-wave interactions in a Heisenberg ferromagnet²¹, which predicts that the dynamical interaction between the spin waves gives, to leading order, a $T^{5/2}$ behavior:

$$D(T) = D_0 \left\{ 1 - \frac{v_0 \bar{l}^2 \pi}{S} \left(\frac{k_B T}{4\pi D_0} \right)^{5/2} \zeta\left(\frac{5}{2}\right) + \dots \right\}, \quad (1)$$

where v_0 is the volume of the unit cell determined by nearest neighbors, S is the average value of the manganese spin, and $\zeta(\frac{5}{2})$ is the Riemann zeta integral. \bar{l}^2 is the moment defined by $\bar{l}^n = \frac{S}{3D} \{ \sum l^{n+2} J(l) \}$ which gives information about the range of the exchange interaction. The solid curves in Fig. 5(b) are fits to Eq. 1, and are in good agreement with the experimental data for temperatures up to 200 K, surprisingly close to T_c . The fitted values of \bar{l}^2 give $\sqrt{\bar{l}^2}_{010} = (2.37 \pm 0.39)b_0$, and $\sqrt{\bar{l}^2}_{001} = (2.56 \pm 0.75)c_0$, where b_0 and c_0 are here the distances to the nearest neighbors ($\simeq 3.896 \text{ \AA}$), and indicate that the exchange interaction extends significantly beyond nearest neighbors in both directions. For $T > 200$ K the experimentally measured values of D depart from the leading order $T^{5/2}$ dependence as expected, having rather a power law behavior (dashed curves) and appearing to collapse as $T \rightarrow T_c$.

In the course of these measurements we have noticed that the central quasielastic peak has a strong temperature dependence, while typically the central peak originates from weak temperature-independent nuclear incoherent scattering. Figure 6(a) shows two magnetic inelastic spectra collected at 210 and 220 K, and reduced wave vector $q = 0.125$ away from the (0 0 2) reciprocal point. A flat background of 0.6 counts plus an elastic incoherent nuclear peak of 100 counts, measured at 10 K, have been subtracted from these data. We can clearly see the development of the quasielastic component, comparable in intensity to the spin waves, and the strength of this scattering is shown in Fig. 6(b) as a function of temperature. We observe a significant intensity starting at ~ 210 K (~ 25 K below T_c), and the scattering peaks at T_c . At and above T_c all the scatter-

ing is quasielastic. The appearance in the ferromagnetic phase of a quasielastic component comparable in intensity to the spin waves was first observed on Ca-doped polycrystalline samples⁸ and it has been suggested that it is associated with the localization of the e_g electrons on the $\text{Mn}^{3+}/\text{Mn}^{4+}$ lattice, and that it may be related to the formation of spin polarons in the system²². We have observed a similar anomalous behavior of the central peak in the strongly-doped system $\text{La}_{0.70}\text{Sr}_{0.30}\text{MnO}_3$,²³ but not in the pyrochlore $\text{Tl}_2\text{Mn}_2\text{O}_7$.²⁴ It thus appears that the coexistence of spin-wave excitations and spin diffusion is a common characteristic for many perovskite manganites, and it raises the question about its relevance for the colossal magnetoresistance property of the perovskite manganites.

b) Large wave vector regime

One of the major open questions in the field of doped manganites concerns the appropriate spin Hamiltonian in the ordered state. The simplest candidate is the Heisenberg form with couplings J_{ij} between pairs of localized spins at sites \mathbf{R}_i and \mathbf{R}_j , $H = -\sum_{ij} J_{ij} \mathbf{S}_i \cdot \mathbf{S}_j$. The double exchange model in the limit of large Hund's coupling²⁵ gives the same (cosine-band) dispersion relation as a ferromagnetic Heisenberg model with nearest-neighbor spin exchanges, but is expressed in terms of different parameters (electron transfer energy t and Hund's coupling J_H , $J_H/t \rightarrow \infty$ in this case). In the case of J_H finite, however, the double exchange model does not provide an analytical form of the dispersion relation that can be readily compared to the experimental data. For simplicity reasons, we have compared our data to the Heisenberg model.

The spin-wave excitations have been measured to the zone boundary, and the dispersion curves at 10 K for the (0,1,0) and (0,0,1) directions are plotted in Fig. 7. The solid curves are the Heisenberg model with a ferromagnetic nearest-neighbor coupling $J_1 S = 3.55 \pm 0.06$ meV obtained from a fit in which all the data were given the same weight. If we perform a fit giving more weight to the low- q data (where the spin-wave excitations are well defined and the energies have been obtained from high-resolution measurements), we obtain $J_1 S = 3.00 \pm 0.02$ meV, and the result is depicted by the dashed curves. The magnon bandwidth in a double exchange model for large Hund's coupling²⁵ $J_H \rightarrow \infty$ would then be $E_{SW} \equiv 24J_1 S = 85.2$ meV. Using a spherical free-electron model Fermi surface, we estimate an electron transfer energy $t = 0.11$ eV. The overall agreement is reasonable in the first case (solid curves), except for a region of intermediate energies below $q=0.5$, while in the second case (dashed curves) the agreement is excellent at low energies, but becomes poor for $q \geq 0.5$. In the (0,0,1) direction we see the manifestation of an additional feature: the opening of a small gap in the spin-wave spectrum at $q = 0.5$, which is likely related to the presence of the odd-integer superlattice peaks at (0 0 l) that appear

below $T_{CA} = 205$ K. It would be interesting to check if this gap goes away above T_{CA} , when the system recovers the exact FM structure. Unfortunately, measuring spin waves above 100 K proves to be difficult in this wave vector regime because, as we discuss below, raising the temperature dramatically increases the spin-wave damping to the point that the larger- q magnons become ill defined for temperatures in the range of $T_{CA} \sim 205$ K.

The overall agreement between the calculated and observed dispersion relation might suggest that the Heisenberg model, or a single-band double exchange model, provides a good description of the spin dynamics of the manganite systems⁹. However, in both models the magnons in the ground state are eigenstates of the system. The *observed* magnetic excitations, interestingly enough, develop large intrinsic linewidths with increasing q , even at low temperatures. Figures 8(a), (b) and (c) show for comparison energy scans at different q -vectors along (0,1,0) measured at 10 K, well below T_C (235 K). The instrumental energy resolution (taking into account the slope of the measured dispersion relation) is 1.1 meV, 3.1 meV, 5.6 meV and 5.9 meV at $q = 0.2, 0.3, 0.6$ and 1.0, respectively, while the observed widths are 2.4, 4.9, 28.8, and 46.2 meV, respectively. To obtain quantitative linewidths, all the data have been fit to a convolution of the instrumental resolution function with the spin-wave cross section. For the very large linewidths found at large q , it is important to correct the data for the instrumental background, which is the sum of the sample background, the fast neutron background and the angle-dependent background for small scattering angles (which represented a real problem only for scattering angles $< 15^\circ$). The fast neutron background (dependent on the counting time which can be different at different energy transfers) and the angle-dependent background have been determined by misorienting the analyzer crystal by 5° , and then this background has been subtracted from the data. The Q -independent sample background has been kept fixed in the fits. At each Q , we have scanned a wide energy range to determine the background. The intrinsic linewidths obtained from the fits, assuming a damped harmonic oscillator spectral weight function²⁶, are shown in Fig. 9(a). At the zone boundary in the (0,1,0) direction the damping of the magnetic excitation is ~ 47 meV, comparable to the energy of the excitation, while the resolution width is 5.9 meV. Note that there are significant linewidths at relatively small q as well, but these are dwarfed by the huge widths observed as one proceeds towards the zone boundary. The most likely explanation for the observed damping is a strong magnon-electron interaction due to the itinerant nature of the e_g electrons associated with the electron hopping and double-exchange mechanism. However, in a simple single-band double exchange model the ground state is fully polarized, and the magnon-electron interaction is forbidden by symmetry. This means that the single-particle Stoner-like excitations have a gap due to the energy difference between the up-electron and down-

electron bands (case of a strong ferromagnet). Therefore, the continuum of Stoner modes is in a higher energy region of the spin excitation spectrum, and the low-lying spin wave excitations should be well-defined. Only at finite temperature does a gapless mode of Stoner excitations appear, and this is expected to have a strong damping effect on the spin wave excitations near the zone boundary²⁵. The presence of the small superlattice peaks might also have an effect on the magnon linewidths by breaking the half-metallic symmetry, but it seems very unlikely that this could provide an explanation for these extraordinarily large linewidths at large q . Another possible contribution to the spin-wave damping could come from an alloy effect related to the random distribution of Mn³⁺ and Mn⁴⁺ ions and consequent distribution of exchange interactions, but typically the linewidths due to alloying are quite modest and not strongly anisotropic. Macroscopic inhomogeneities of the sample are ruled out since the magnetic and structural transitions are observed to be sharp. Measurements in the (0,0,1) direction, on the other hand, reveal only modest linewidths for these spin waves, as also shown in Fig. 9(a), and similar to those observed very recently by Hwang et al. in Pr_{0.63}Sr_{0.37}MnO₃.²⁷ The strong damping and its directionality that we observe suggests that hybridization effects in a multiband model must be included in the description of these materials to quantitatively explain the spin dynamics, similar to conventional itinerant electron systems²⁸.

As we mentioned before, there are significant linewidths at relatively small q as well. In the long wavelength regime the linewidths in spin wave theory, due to spin wave-spin wave interactions, are expected to follow $\Gamma(q, T) \propto q^4 [T \ln(kT/E_{sw})]^2$. Figure 9(b) shows the experimentally observed spin-wave linewidths for La_{0.85}Sr_{0.15}MnO₃ for $q \leq 0.25 \text{ \AA}^{-1}$ and for temperatures between 10 and 230 K. We see that the points (solid circles) for $q \leq 0.16 \text{ \AA}^{-1}$ fall quite close to a single universal curve. This indicates that spin wave interactions dominate the linewidths in this regime. At higher q , represented by the open squares in this figure, the data deviate strongly from the expected straight line, and are clearly more strongly damped, even at low temperatures. This is an interesting result in the following sense: The $q^4 [T \ln(kT/E_{sw})]^2$ dependence predicted by the linear spin wave theory is the leading-order behavior expected only in the small- q regime. For higher q , this relation overestimates the observed linewidths, *i.e.* observed linewidths plotted vs. $q^4 [T \ln(kT/E_{sw})]^2$ are expected to lie underneath the straight line. Our results show that the linear spin wave theory relation holds up to $q \simeq 0.16 \text{ \AA}^{-1}$, while for higher q values the linewidths are found to sit *above* the expected straight line, not below. We remark that for larger q ($> 0.26 \text{ \AA}^{-1}$) the linewidths are too large to be included on the plot.

We finally note that increasing the temperature also has a strong effect on the spin-wave damping. At $T = 50$ K, still well below T_C , the zone-boundary magnetic exci-

tation appears to be the same as at 10 K, but at 100 K it broadens to the point of being ill defined (with this resolution), as can be seen in Fig. 8(d). This behavior contrasts markedly with the expectations for a conventional localized-spin ferromagnet, and indicates that there are additional strongly temperature-dependent contributions to the spin-wave damping. The leading-order spin wave damping in the double-exchange model is proportional to $(1 - m^2)$, where m is the reduced magnetization²⁹, and at this low a temperature the expected temperature dependence again appears to be too small to explain these observations. A quantitative description of the spin wave damping as a function of wave vector and temperature in these materials represents a theoretical challenge.

DISCUSSION

A mean-field calculation gives for the Curie temperature of a localized ferromagnet a value $4J_1S(S + 1)$. If we use for S the mean spin on the manganese ions, $S = \frac{3}{2}x + 2(1 - x)$, we calculate a mean field value $T_C^{MF} = 482$ K. This is more than double the experimentally measured value. But it is well known that fluctuations reduce the Curie temperature even for three-dimensional local moment ferromagnets. In particular, for the simple cubic nearest-neighbor Heisenberg ferromagnet, fluctuations reduce T_C to $J_1[2.90S(S + 1) - 0.36]$.³⁰ We evaluate this quantity to be 341 K, still 45% larger than the measured value of 235 K. In other words, the Curie temperature is inconsistent with the magnon bandwidth $E_{SW} \equiv 24J_1S$. For La_{0.85}Sr_{0.15}MnO₃ we find that the magnon bandwidth is significantly (about a factor of two) larger than the Curie temperature of 235 K. The large value of J_1 determined from our neutron scattering measurements of the spin wave spectrum indicates that this system is not localized, but has itinerant character. The renormalization of T_C from the mean-field value in a Heisenberg Hamiltonian (which is appropriate for ferromagnetic insulators or localized spin systems) is considered to be a good measure of the itineracy. An itinerant ferromagnet will have a lower T_C compared to the mean-field value, but will have large values of J , consistent with the present results. A calculation of T_C performed by Furukawa within the double exchange model (the Kondo lattice model with ferromagnetic couplings) in the infinite-dimensional approach³¹ reproduces the experimental result for La_{0.85}Sr_{0.15}MnO₃ when using a bandwidth of the itinerant e_g electrons $W = 1.05$ eV and a Hund's coupling $J_H = 4.2$ eV. This value of W gives a large value of the electron transfer energy $t \equiv W/6 = 0.175$ eV, which is probably a more accurate value than the one we have previously estimated from the magnon bandwidth using a spherical free-electron model Fermi surface.

This manifestation of the itinerant character of the spin system and the isotropy of the exchange interactions demonstrate that the dimensional crossover from the 2D-like planar ferromagnetic in the low doping limit to the

3D isotropic ferromagnetic character takes place at concentrations lower than $x=0.15$, probably $x \sim 0.1$.^{11,12} It is remarkable that the metallic ferromagnetic features in the spin dynamics appear at lower doping concentrations than the compositional insulator-metal transition at $x \sim 0.17$. It is therefore conjectured that the insulator-metal phase boundary would have been located at $x=0.1$ in the $\text{La}_{1-x}\text{Sr}_x\text{MnO}_3$ system, if it were not for the spin canting transition that suppresses the metallic conduction in samples with $0.1 \leq x \leq 0.15$.¹³ It is this itinerant character of the e_g electrons, viewed as a hopping conduction channel implemented by the scattering of a high-energy spin wave, that may be responsible for the anomalous spin-wave damping effects observed in this system.

Research at the University of Maryland is supported by the NSF under Grant DMR 97-01339 and by the NSF-MRSEC, DMR 96-32521. Experiments on the NG-5 spectrometer at the NIST Research Reactor are supported by the NSF under Agreement No. DMR 94-23101.

- ²² J. W. Lynn et al., *J. Appl. Phys.* **81**, 5488 (1997).
- ²³ L. Vasiliu-Doloc et al., *J. Appl. Phys.* **83**, 7342 (1998).
- ²⁴ J. W. Lynn, L. Vasiliu-Doloc, M. A. Subramanian, *Phys. Rev. Lett.* **80**, 4582 (1998).
- ²⁵ N. Furukawa, *J. Phys. Soc. Jap.* **65**, 1174 (1996).
- ²⁶ We have also used a Lorentzian for the assumed spectral weight function, and results are qualitatively the same.
- ²⁷ H. Hwang et al., *Phys. Rev. Lett.* **80**, 1316 (1998).
- ²⁸ See, for example, J. F. Cooke, J. W. Lynn, and H. L. Davis, *Phys. Rev. B* **21**, 4118 (1980).
- ²⁹ N. Furukawa et al., *Physica B* **241-243**, (1998) (in press).
- ³⁰ G. S. Rushbrooke et al., in *Phase Transitions and Critical Phenomena*, edited by C. Domb and m. S. Green (Academic, New York, 1974).
- ³¹ N. Furukawa, *J. Phys. Soc. Jap.* **64**, 2754 (1995).

- ¹ For early literature, see G. H. Jonker and J. H. van Santen, *Physica* **16**, 337 (1950); E. O. Wollan and W. C. Koehler, *Phys. Rev.* **100**, 545 (1955); G. H. Jonker, *Physica* **22**, 707 (1956); J. B. Goodenough, *Phys. Rev.* **100**, 564 (1955).
- ² Y. Tokura et al., *J. Phys. Soc. Jpn.* **63**, 3931 (1994).
- ³ K. Chabara et al., *Appl. Phys. Lett.* **63**, 1990 (1993); S. Jin et al., *Science* **264**, 413 (1994).
- ⁴ C. Zener, *Phys. Rev.* **82**, 403 (1951); P. W. Anderson and H. Hasegawa, *Phys. Rev.* **100**, 675 (1955); P. G. de Gennes, *Phys. Rev.* **100**, 564 (1955).
- ⁵ A. J. Millis, P. B. Littlewood, and B. I. Shraiman, *Phys. Rev. Lett.* **74**, 5144 (1995); A. J. Millis, *Phys. Rev. B* **55**, 6405 (1997).
- ⁶ M. C. Martin et al., *Phys. Rev. B* **53**, 14 285 (1996).
- ⁷ A. H. Moudden et al., *Czech. J. Phys.* **46**, 2163 (1996).
- ⁸ J. W. Lynn et al., *Phys. Rev. Lett.* **76**, 4046 (1996).
- ⁹ T. G. Perring et al., *Phys. Rev. Lett.* **77**, 711 (1996).
- ¹⁰ J. A. Fernandez-Baca et al., *Phys. Rev. Lett.* **80**, 4012 (1998).
- ¹¹ A. H. Moudden et al., *Physica B* **234-236**, 859 (1997).
- ¹² K. Hirota et al., *J. Phys. Soc. Jpn.* **65**, 3736 (1996).
- ¹³ H. Kawano et al., *Phys. Rev. B* **53**, 2202 (1996).
- ¹⁴ P. Wochner, A. H. Moudden, L. Vasiliu-Doloc, J. W. Lynn, A. Revcolevschi, in preparation.
- ¹⁵ L. Vasiliu-Doloc et al., *J. Appl. Phys.* **81**, 5491 (1997).
- ¹⁶ L. Vasiliu-Doloc et al., *Bull. Am. Phys. Soc.* **41**, 529 (1996); *ibid.* **42**, 264 (1997).
- ¹⁷ A. Urushibara et al., *Phys. Rev. B* **51**, 14103 (1995).
- ¹⁸ A. Anane et al., *J. Phys.: Condens. Matter* **7**, 7015 (1995).
- ¹⁹ H. Kawano et al., *Phys. Rev. B* **53**, R14709 (1996).
- ²⁰ Y. Yamada et al., *Phys. Rev. Lett.* **77**, 904 (1996).
- ²¹ D. C. Mattis, *The theory of magnetism*, Springer-Verlag, Heidelberg, 1981.

FIGURE CAPTIONS

FIG. 1 (a) Temperature dependence of the (1 2 0) nuclear Bragg reflection which is allowed only in the orthorhombic structure. The system undergoes an abrupt R-to-O' structural phase transition at $T_S \simeq 360$ K. The (1 2 0) reflection reacts both at T_C and T_{CA} , indicating a coupling between the lattice and the magnetic system. (b) Temperature dependence of the (0 2 0) ferromagnetic peak and (0 0 3) AF peak. Note that the onset of AF intensity occurs at $T_{CA} < T_C$ and coincides with a break in the ferromagnetic intensity consistent with a reduction in the FM moment due to a canting of spins. Note also the factor of ten difference in intensity scales, with the (0 0 3) intensity being about 40 times weaker than the (0 2 0) intensity.

FIG. 2 Temperature dependence of the profile of the (0 0 3) reflection. There is no significant scattering at 215 K ($< T_C = 235$ K).

FIG. 3 Schematic illustration of the magnetic structure of $\text{La}_{0.85}\text{Sr}_{0.15}\text{MnO}_3$: (a) purely ferromagnetic for $T_{CA} \leq T \leq T_C$; (b) spin canted below T_{CA} . The cant angle is small, $(9.4^\circ \pm 0.8^\circ)$, resulting in a small antiferromagnetic component.

FIG. 4 Temperature dependence of the a and b lattice parameters showing the strong reaction of the lattice at T_C and T_{CA} . a and b are very different above T_C (the system is in the orthorhombic O' phase), then the ferromagnetism drastically suppresses the static lattice distortion and a and b become almost equal at T_C , but next the precursor effects of the phase transition at T_{CA} distort the lattice once more, before releasing the lattice distortion almost completely below T_{CA} . Due to the uncertainty in identifying a and b from single-crystal diffraction on a twinned sample, the situation described in (b) may be realized, where there is a crossover between a and b at T_C .

FIG. 5 (a) Spin-wave dispersion along (0,0,1) in the long wavelength limit at 10 K (open circles) and 220 K (closed circles). Solid curves are fits to $E = E_0 + Dq^2$. (b) The spin-wave stiffness coefficient in the (0,1,0) (closed circles) and (0,0,1) (open circles) directions vs. T . The solid curves are fits to Eq. (1). For $T > 200$ K the measured values of D depart from the $T^{5/2}$ dependence and the dashed curves are fits to a power law.

FIG. 6 (a) Magnetic inelastic spectra collected at 210 and 220 K, and a reduced wave vector $q = (0, 0, 0.125)$. A flat background of 0.6 counts plus an elastic incoherent nuclear peak of 100 counts, measured at 10 K, have been subtracted from these data. The dominant effect is the development of a strong quasielastic component in the spectrum. (b) Integrated intensity versus temperature for the central peak at $q = (0, 0, 0.15)$. The quasielastic scattering starts increasing in intensity well below T_C . Above T_C , all the scattering in this range of q is quasielastic.

FIG. 7. Spin-wave dispersion along (0,1,0) and (0,0,1) measured to the zone boundary at 10 K. The solid curves

are fits to a Heisenberg model with $J_1S = 3.55 \pm 0.06$ meV obtained by giving all the data the same weight. The dashed curves are fits to a Heisenberg model with $J_1S = 3.00 \pm 0.02$ meV obtained by favoring the low- q data.

FIG. 8. Magnetic inelastic spectra collected at 10 K for reduced wave vectors (a) $q = 0.2$ (open circles) and $q = 0.3$ (closed circles), (b) $q = 0.6$, (c) $q = 1.0$ in the (0,1,0) direction. The magnetic excitations are increasingly broader with q . The solid curves are fits to a convolution of the instrumental resolution function with the spin-wave cross section. The horizontal arrows indicate the width of the instrumental energy resolution E_R . (d) Energy scan at $q = 1.0$ at 100 K, still well below T_C , showing that the magnetic excitation at the zone boundary has broadened beyond recognition (with this resolution).

FIG. 9 (a) Intrinsic spin-wave linewidths versus q at 10 K along the (0,1,0) (closed circles) and along the (0,0,1) direction (open squares). The damping at the zone boundary in the (0,1,0) direction is ~ 47 meV, comparable to the spin-wave energy, but it is smaller in the (0,0,1) direction. (b) Intrinsic spin-wave linewidths versus the expected (q, T) dependence in linear spin wave theory. Linewidths of spin waves for $q \leq 0.16 \text{ \AA}^{-1}$ (closed circles) fall quite close to a single universal curve, whereas linewidths for $0.16 < q < 0.25 \text{ \AA}^{-1}$ (open squares) deviate significantly from the expected straight line. The low temperature linewidths at higher q are off scale on this plot.

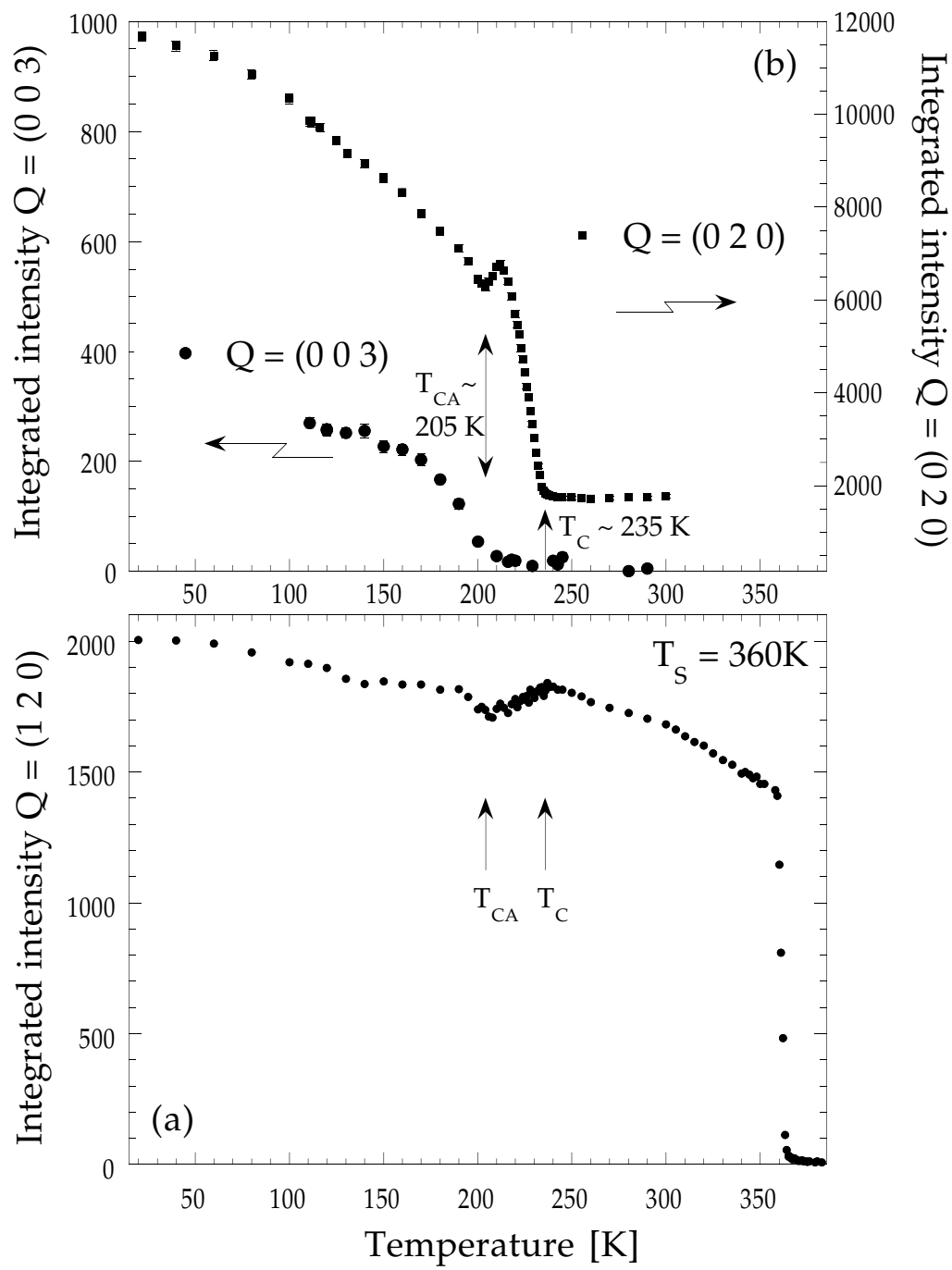


FIG. 1: L. Vasiliu-Doloc et al.

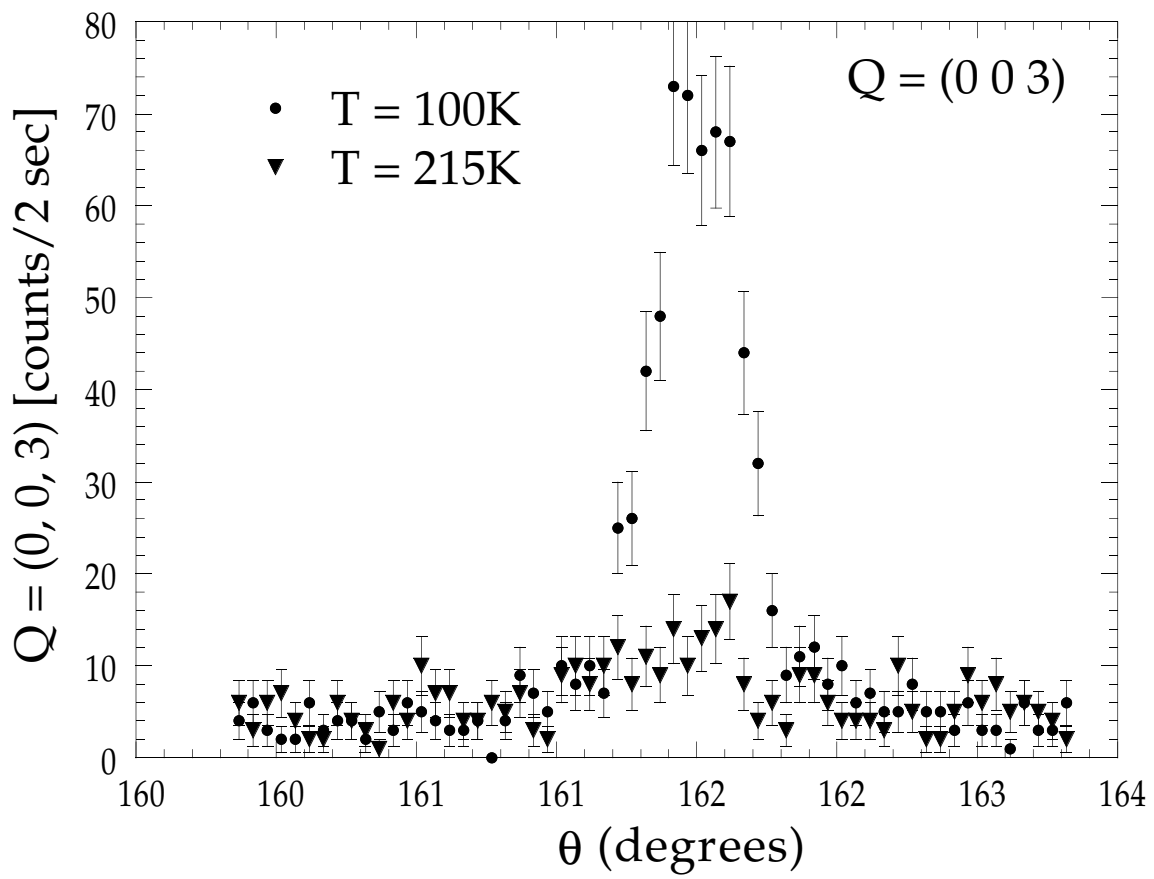


FIG. 2: L. Vasiliu-Doloc et al.

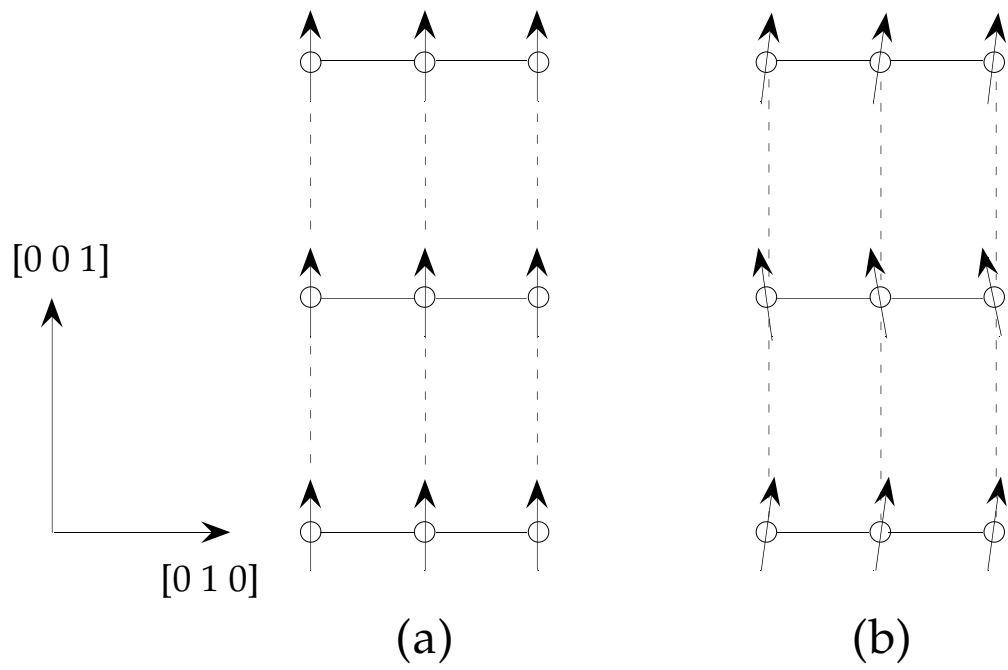


FIG. 3: L. Vasiliu-Doloc et al.

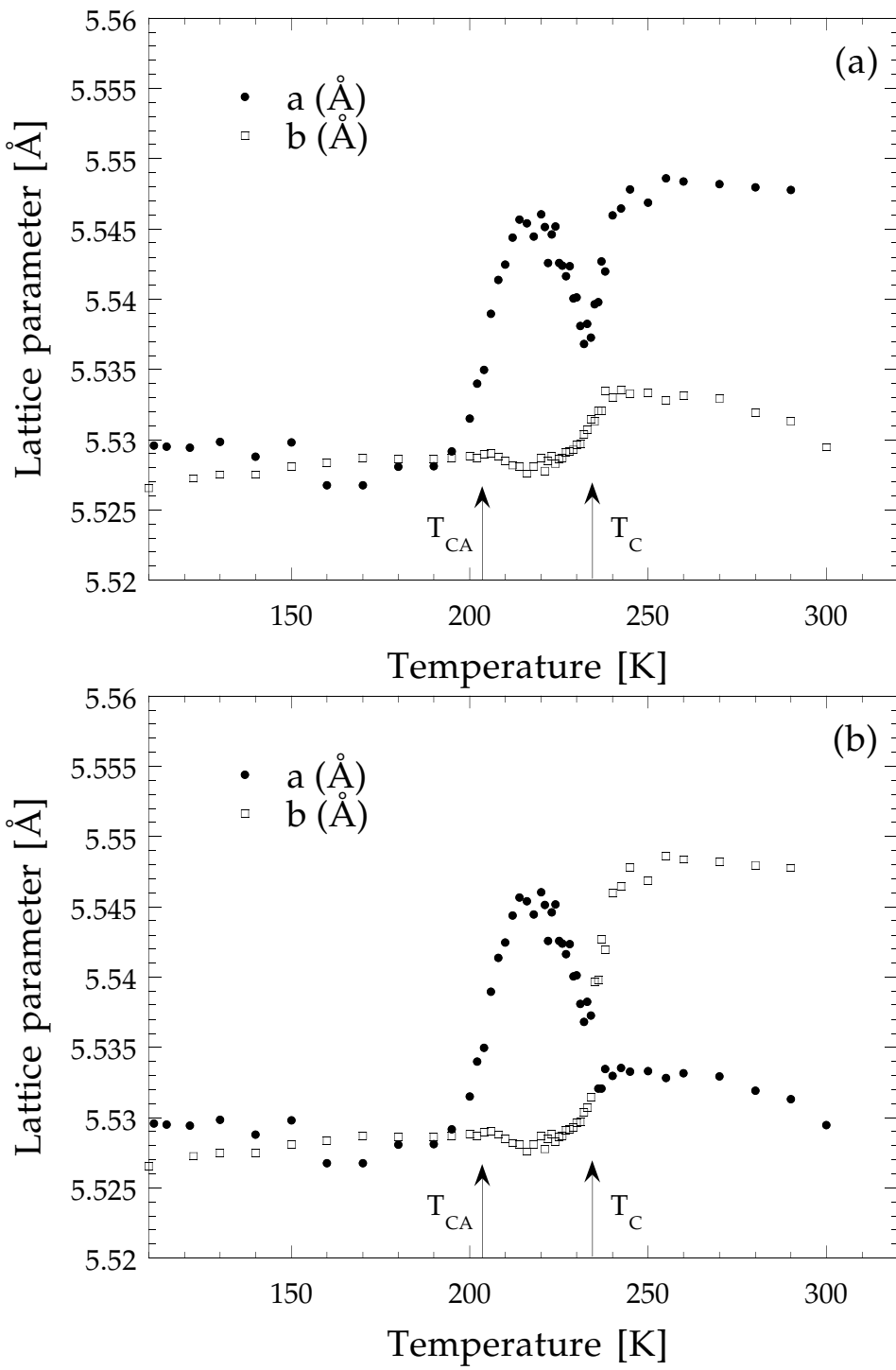


FIG. 4: L. Vasiliu-Doloc et al.

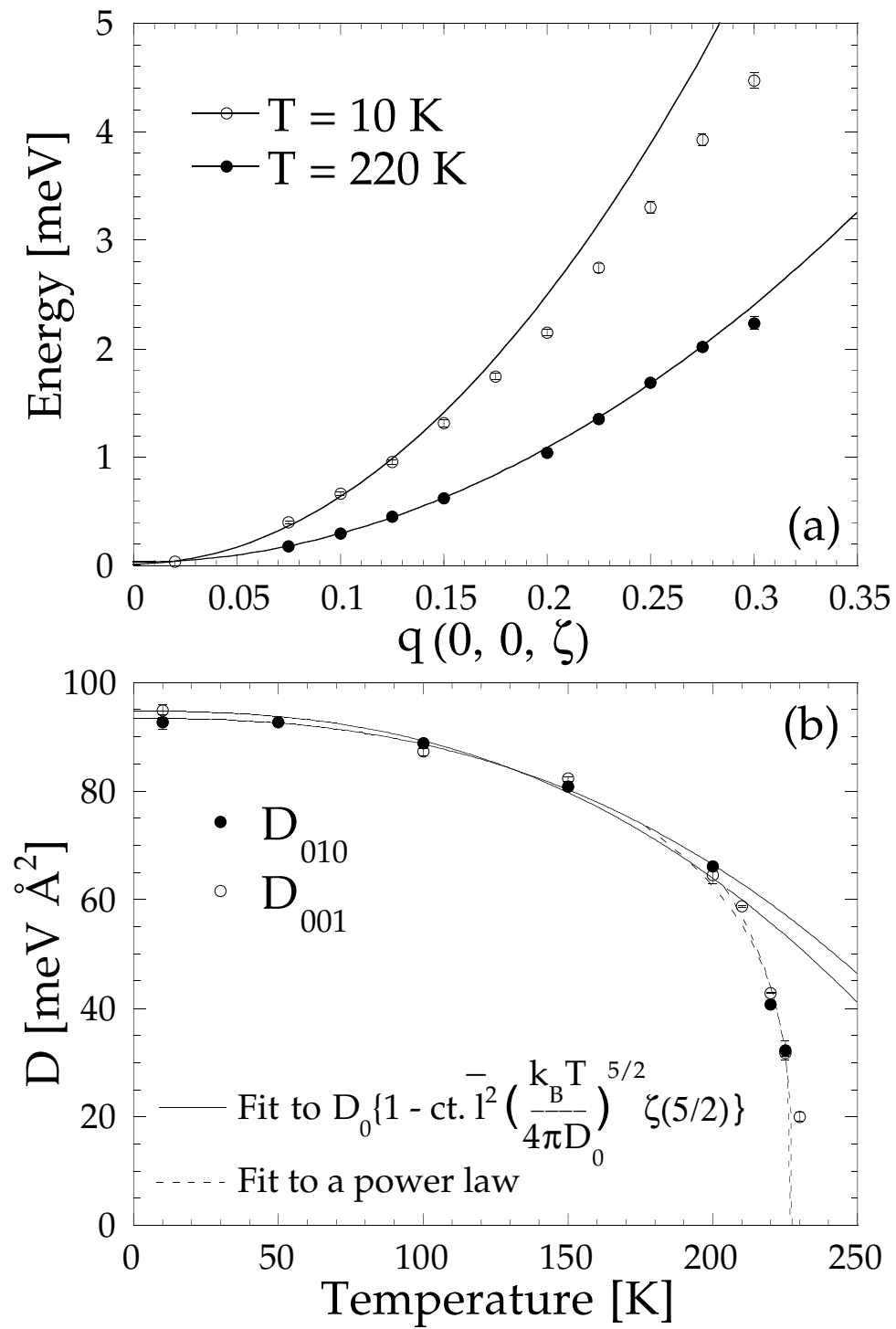


FIG. 5: L. Vasiliu-Doloc et al.

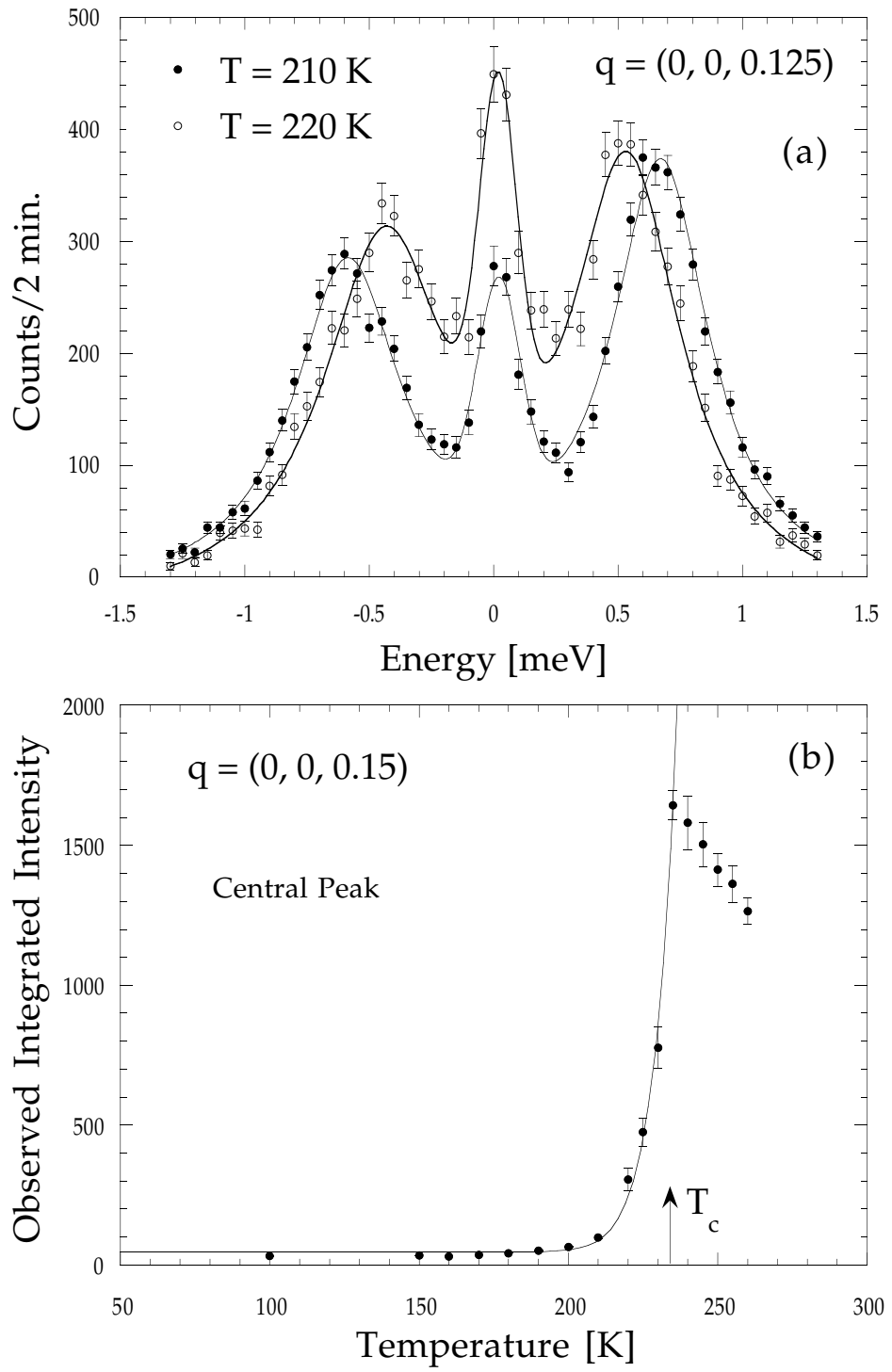


FIG. 6: L. Vasiliu-Doloc et al.

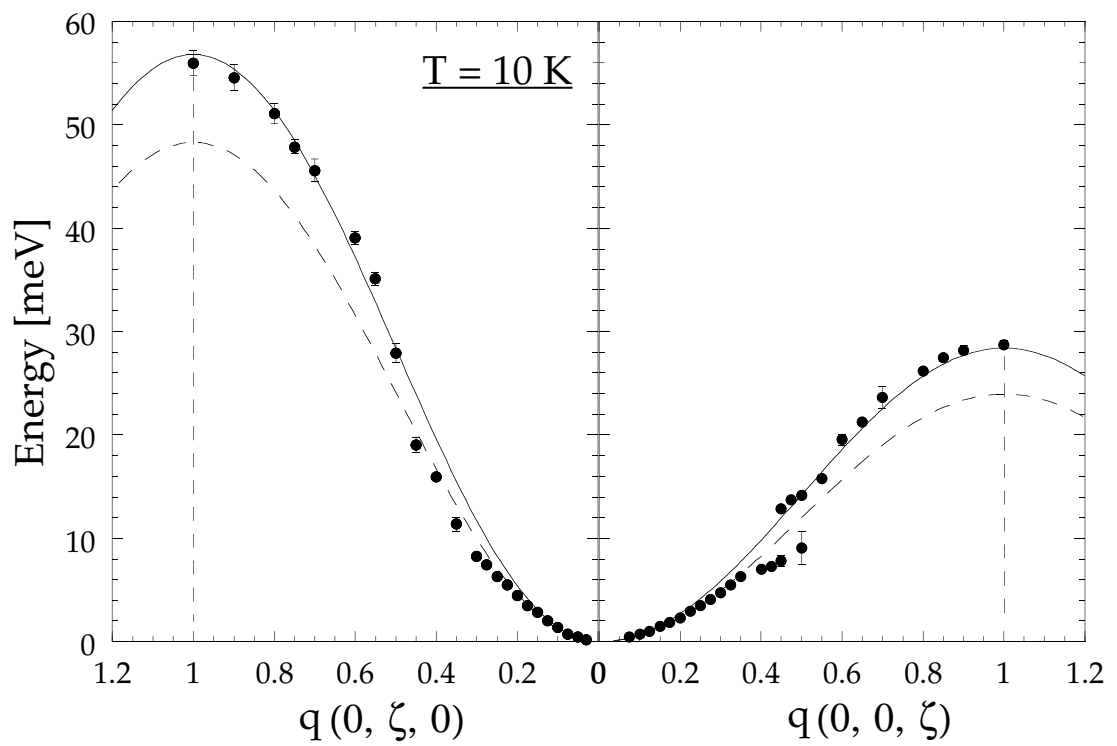


FIG. 7: L. Vasiliu-Doloc et al.

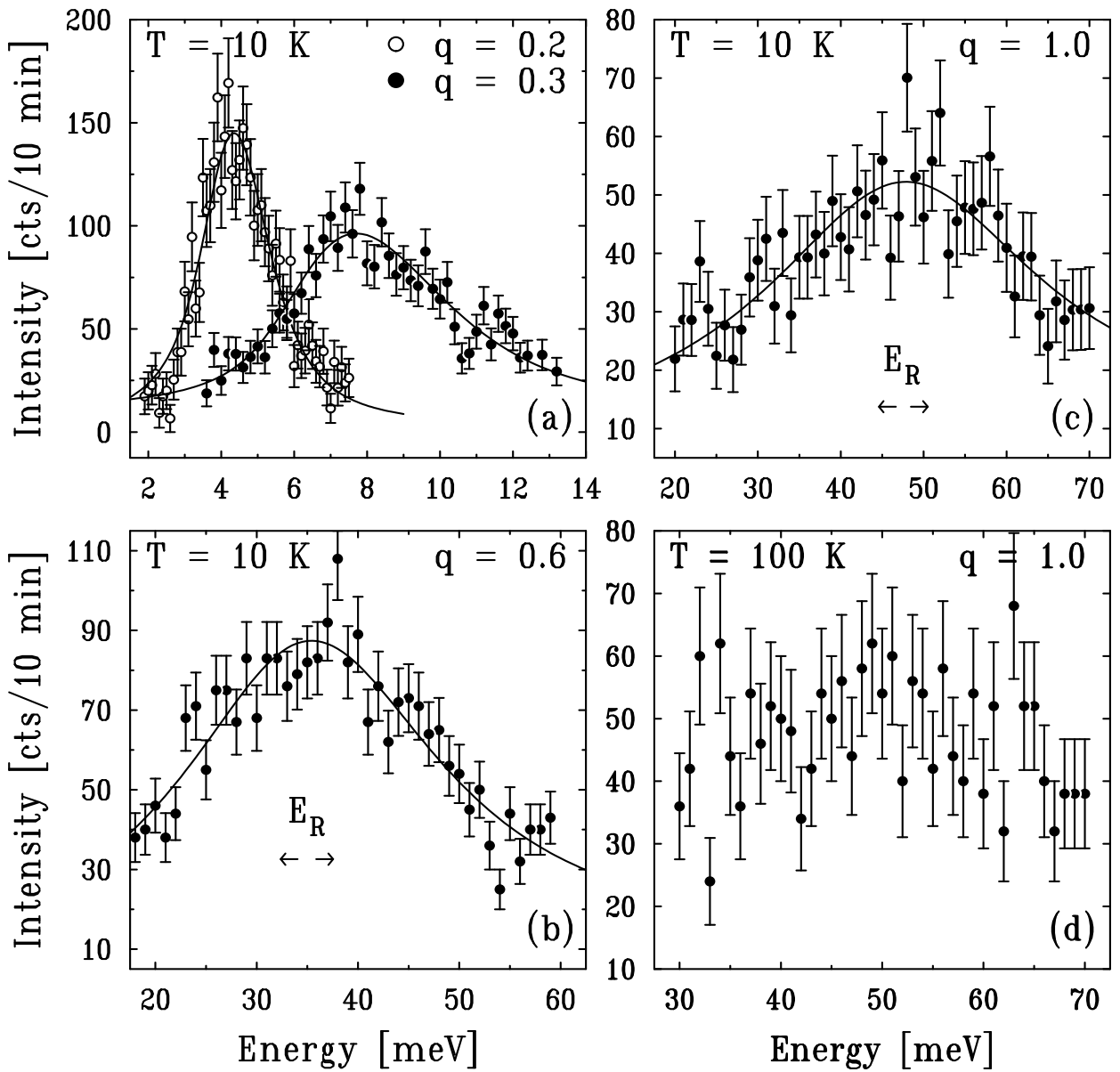


FIG. 8: L. Vasiliu-Doloc et al.

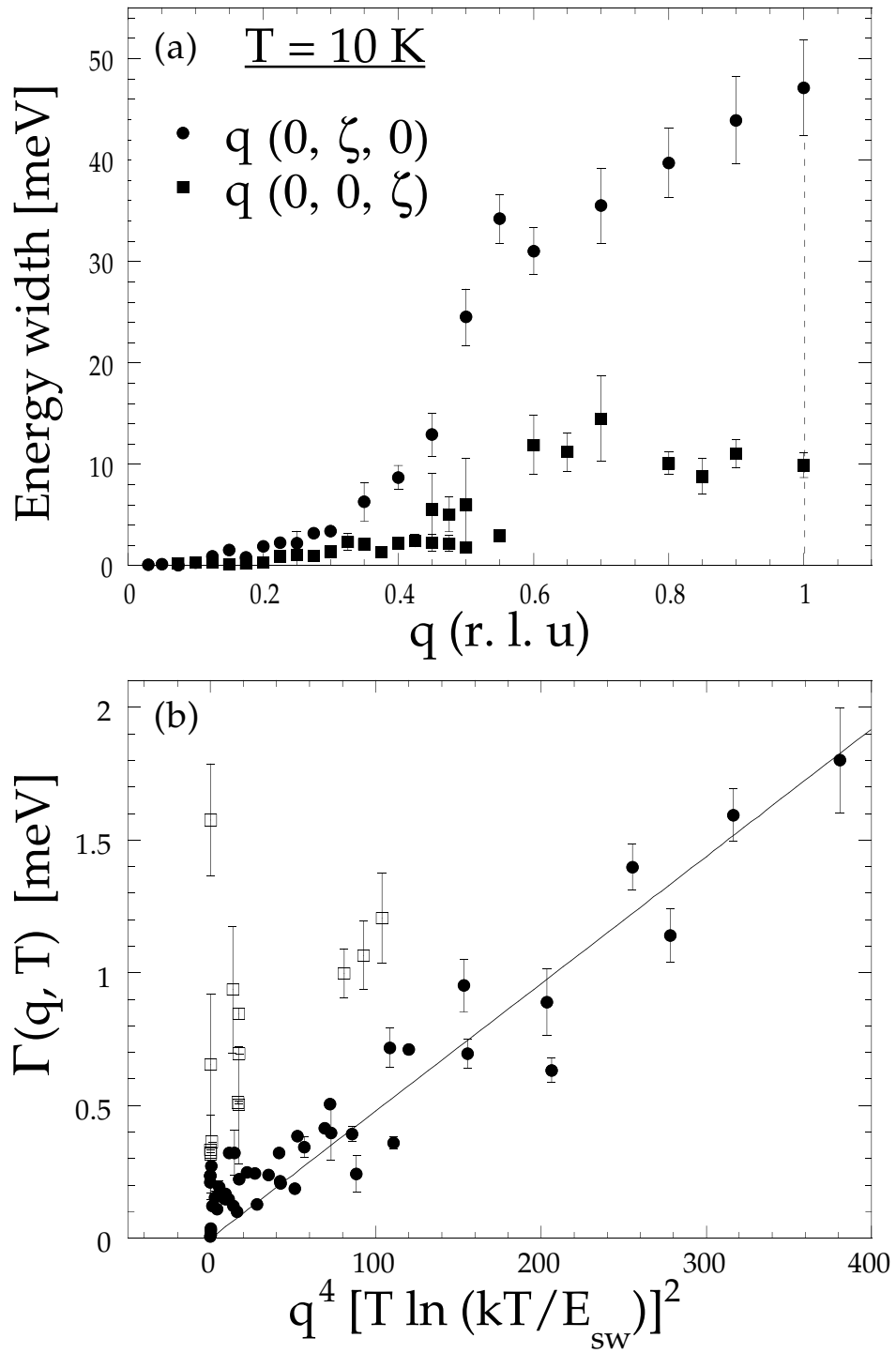


FIG. 9: L. Vasiliu-Doloc et al.